Eur. Phys. J. Plus (2022) 137:911
https://doi.org/10.1140/epjp/s13360-022-03135-2

THE EUROPEAN PHYSICAL JOURNAL PLUS

Regular Article

Effect of lamination angle on control performance for composite beams subject to galloping-based flow-induced vibration

Sinan Basaran[1,a], **Fevzi Cakmak Bolat**[2]

[1] Department of Mechanical Engineering, Bilecik Seyh Edebali University, 11230 Bilecik, Turkey
[2] Department of Mechanical Engineering, Bolu Abant İzzet Baysal University, 14280 Bolu, Turkey

Received: 11 February 2022 / Accepted: 1 August 2022

Abstract In this study, the active vibration control system design of a composite beam with three different lamination angles under forced vibration was investigated. The produced composite beam lamination angles have been selected as $\{0°, 90°, 0°, 90°\}_s$, $\{-30°, 60°, -30°, 60°\}_s$ and $\{-45°, 45°, -45°, 45°\}_s$ for investigating the vibration characteristic. Different types of bluff-body geometries were attached to the free end of the cantilever composite beams. In this way, the composite beam's vibration amplitudes have more fluctuated with the help of bluff body geometries. Bluff body structures are generally preferred in energy harvesting applications by increasing the vibration in beams. The fact that this structure, which increases the vibration amplitude, is handled in an active vibration control mechanism adds a different novelty to the subject. Flow-induced vibrations were obtained for a particular period by applying air load on it. Two different geometries of bluff bodies were placed in a freestream airflow at a constant speed to trigger and enhance the vibration of the composite beam. The front surface areas of two different bluff bodies exposed to air load are identical. Therefore, the difference in the vibrations characteristics was only affected by the geometrical differences in the lateral areas of the bluff bodies. To demonstrate this situation, the airfoil efficiency was investigated for the bluff body geometries. A piezoelectric patch is attached to the surface of the composite beam, and the vibration control is acquired utilizing the PID control design. As a result of experimental studies, it has been shown that the forced vibrations on the composite structure can be suppressed successfully with the application of the PID control design.

1 Introduction

Composite materials are used extensively in the aviation, robotics, military, and automobile industry due to their high strength and lightweight characteristics. Composite materials can be exposed to vibration due to different external dynamic factors as in all other materials. These undesired vibrations can cause noise and, more importantly, can cause damage to the structures. These vibrations in structural systems can be controlled using piezoelectric materials as actuators [1–5]. In the literature, there are studies aimed at suppressing unwanted vibrations on beam elements with different types of active control methods [6–10]. Takacs et al. used the piezoelectric material in actuator mode by gluing it next to the built-in boundary condition of the beam and used it in sensor mode by bonding another piezoelectric material to the endpoint of the same beam. They have experimentally performed the suppression of vibrations on the cantilever beam using the adaptive model predictive control method [11]. Oveisi and Gudarzi have controlled the geometrically nonlinear cantilever beam vibrations using the adaptive fuzzy method with a piezoelectric actuator [12]. Zhu et al. have controlled piezoelectric-based cantilever beam vibrations with an adaptive feedforward method. Their work has performed time–frequency analysis by adding an equivalent noise signal to their control algorithm designs. The designed controller has suppressed vibrations of unknown multiple frequencies [13]. Sivrioglu et al. have adhered to the piezoelectric patch on a wing element to suppress the vibrations caused by air load. They have used the experimentally and theoretically robust control method in their setup. In their study, the reduction of the structure's frequency amplitudes under the controller's effect and its displacement in time responses have been examined [14].

There are studies available in which different active vibration control methods are applied to suppress vibrations occurring on composite beam structures. Youn et al. have experimentally controlled the vibrations of the composite beam with a piezoelectric patch bonded with the neural network control scheme. They have examined the effects of different thicknesses of the adhesive layer on the natural frequency and compared their control performance [15]. Koroishi et al. have created a smart beam structure by sticking a piezoelectric patch on a composite beam. The vibrations of the smart beam structure have been suppressed with the Kalman-based fuzzy modal control method [16].

Ma and Nejhad, in their work, have suppressed composite beam vibrations with the adaptive PID control method, which has two different feedback structures with the piezoelectric patch. The results of both control methods have been experimentally compared

[a] e-mail: sinan.basaran@bilecik.edu.tr (corresponding author)

Published online: 10 August 2022

[17]. Koroishi et al. have controlled the vibrations of the smart composite structure with the robust control method based on linear matrix inequalities. In their studies, the natural frequencies of the composite structure were determined by the numerical calculation method, and the time and frequency responses were examined [18]. Zheng et al. have proposed a new type of nonlinear suspension based on NiTiNOL-steel wire rope (NiTi-ST) to suppress composite beam vibrations. They have achieved the suppression of composite vibrations with the passive control structure they proposed [19]. Jovanovic et al. have experimentally controlled the vibrations of the piezoelectric composite beam, which has $\{0°/45°/-45°\}_s$ lamination angle with the PID control method. They have modeled the composite structure with the finite element method and analyzed the time responses by trying different configurations of the PID control method [20]. Shakir and Saber have numerically modeled the intelligent composite structure with the commercial finite element program and controlled it theoretically [21]. Varadarajan et al. have created the mathematical model of the intelligent composite beam element with higher-order shear deformation theory. They have controlled the vibrations of the composite structure theoretically using the robust control method over the model they obtained [22].

There are very few experimental studies in the literature regarding the effects of the lamination angle of composite beams on control. Active vibration control responses of composite beams with different angular orientations were not investigated in previous literature studies. When the current studies are examined, it is seen that an active control application has been made on composite beams with a single fiber orientation [23–25]. There is no study on the stiffness of composite beams against the controller by revealing a continuous vibration state under the influence of the air effect. Apart from this, in active vibration control studies, oscillations on the structure are carried out using a shaker. In this study, the effects of a PID controller on the vibration response of beams with different lamination angles were investigated. On the other hand, flow-induced vibrations were obtained from different bluff-body geometries, and control responses against varying aerodynamic forces were analyzed. In this paper, the following topics are briefly reviewed.

- Controlling the vibrations of composite beams with different lamination angles by the PID control method has been investigated.
- The time responses of smart composite beams with different lamination angles for the same PID control design were examined.
- Instead of the usual shaker-like vibration in the literature, more realistic bluff-body geometries were connected to the smart composite beam endpoint, and vibrations were obtained by applying air load to it.
- At the same time, the vibrations created by bluff bodies with different geometric shapes on beams with varying lamination angles and their control performance were investigated.
- Bluff body geometries designed in different geometries are generally used as vibration-increasing elements. In this study, a different approach was taken by examining the active vibration control of different types of bluff bodies.

The rest of the paper is organized as follows: In Sect. 2, system modeling and detailed information on the composite beam are presented. In the same section, the effects of different types of bluff body geometries on vibration are also mentioned. Section 3 gives the information on the control design with the PZT patch actuator and the experimental system setup details. Finally, the experimental results and conclusion are given in the following two sections, respectively.

2 Composite beam with bluff body attachment system specifications and modeling

In this study, active vibration control of thin composite beams with eight layers of different lamination angles is investigated experimentally. A PZT patch has been attached to the composite beam to suppress the aeroelastic structure vibrations. The lamination angles of the beams are $\{0°, 90°, 0°, 90°\}_s$, $\{-30°, 60°, -30°, 60°\}_s$ and $\{-45°, 45°, -45°, 45°\}_s$ as seen in Fig. 1. The mechanical and physical properties of composite and piezoelectric materials are given in Table 1.

Using a force gauge stiffness values, all the composite beams were determined experimentally. Bending vibration will occur on composite beams due to boundary conditions resulting from the flow-induced dynamic effect. The natural frequency values of composite beams with three different lamination angles are calculated using the finite element method and given in Table 2. In these

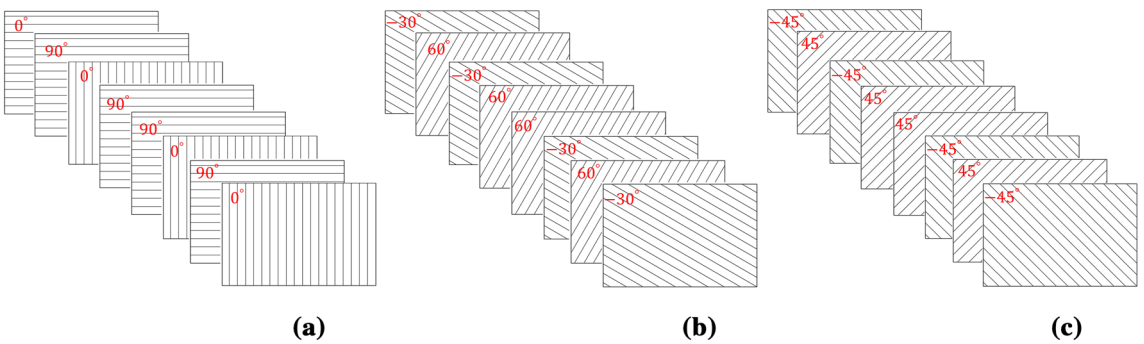

Fig. 1 Angular orientation of the composite beams **a** $\{0°, 90°, 0°, 90°\}_s$ **b** $\{-30°, 60°, -30°, 60°\}_s$ **c** $\{-45°, 45°, -45°, 45°\}_s$

Table 1 Properties of the PZT path and composite beams

Property (unit)	Value
Thickness (m) × width (m)	0.002×0.05
Length (m)	0.22
Elasticity along with the first reinforcing fiber (GPa)	21.3
Elasticity along with the second reinforcing fiber (GPa)	21.1
Poisson's ratio	0.161
Shear modulus (GPa)	3.003
Density (kg m^{-3})	1771.21
Length of the PZT patch (m)	0.050
Width of the PZT patch (m)	0.030
The thickness of the PZT patch (m)	0.0005
Density of the PZT (kg m^{-3})	7800
Young's modulus of the PZT patch (GPa)	6.2

Table 2 Natural frequencies of the composite beams

Mode no.	$\{0°, 90°, 0°, 90°\}_s$ with bluff body mass (Hz)	$\{-30°, 60°, -30°, 60°\}_s$ with bluff-body mass (Hz)	$\{-45°, 45°, -45°, 45°\}_s$ with bluff-body mass (Hz)
1	13.6637	10.5091	9.8727
2	120.6997	92.9411	87.5394
3	369.4451	287.7628	271.9731

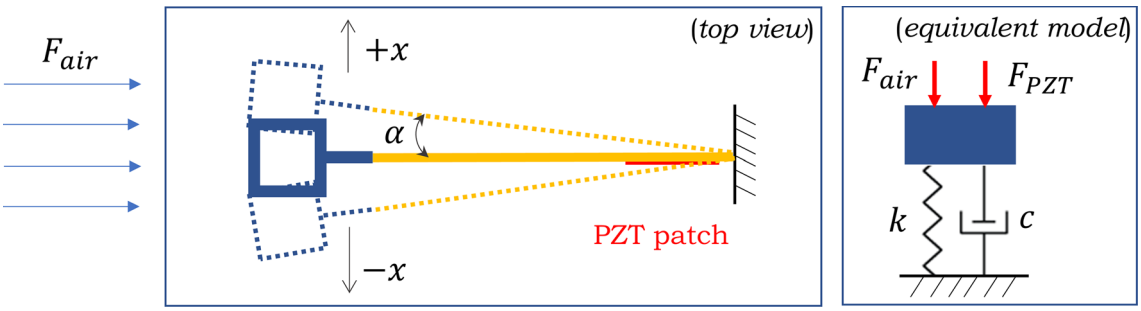

Fig. 2 Schematic representation of the PZT-composite beam smart system and its equivalent dynamical model

calculations, the masses of the bluff body geometries attached to the end of the composite beam are also considered. The masses of the bluff bodies are 0.026 (kg) for triangular-shaped and square-shaped bluff bodies. Experimentally measured values are $K = 1.5122 \times 10^3$ (N/m) for $\{0°, 90°, 0°, 90°\}_s$ composite beam, $K = 1.303 \times 10^3$ (N/m) for $\{-30°, 60°, -30°, 60°\}_s$ composite beam, and $K = 1.152 \times 10^3$ (N/m) for $\{-45°, 45°, -45°, -45°\}_s$ composite beam. These values coincide with the natural frequency values in Table 2 obtained by the numerical method.

Two different types of bluff-body geometries are attached to the free end of these cantilever composite beams to obtain flow-induced vibration in a regular regime. As shown in the schematic representation in Fig. 2, with the application of air load on the bluff-body geometries, vibration occurs as a result of aerodynamic effects (vortex) on the cantilever composite beam. Here, one of the most important parameters of the control response is the stiffness value of the composite beams. Another critical parameter for the control performance is the bluff-body physical geometric shape (Fig. 3).

The cantilever composite beam element, which has internal damping and known mass and rigidity properties, is subjected to forced vibration due to airflow. The equation of motion of the cantilever composite beam element forced due to air load and controlled by a PZT element can be written as follows.

$$M\ddot{x}(t) + C\dot{x}(t) + Kx(t) = F_{\text{pzt}}(t) + F_{\text{air}}(t) \tag{1}$$

where F_{pzt} is the control force, M is the mass matrix, C is the damping matrix, and K is the stiffness matrix. Air force on the bluff body F_{air} is expressed as follows [26].

$$F_{\text{air}} = \frac{1}{2}\rho V^2 D\left[a_1\frac{\dot{x}}{V} + a_3\left(\frac{\dot{x}}{V}\right)^3\right] \tag{2}$$

Here ρ, A, V, D represent the air density, surface area, air velocity, and the aerodynamic force component, respectively.

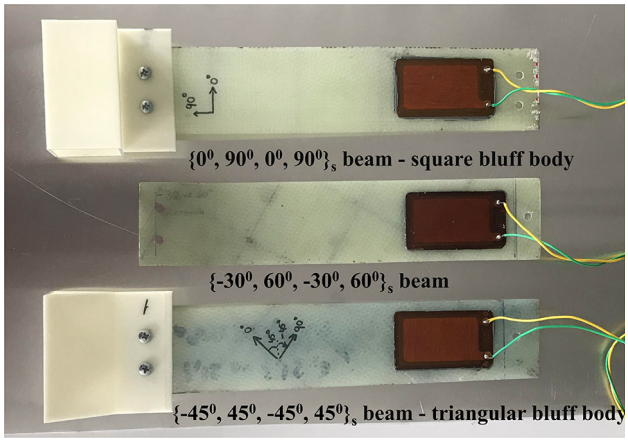

Fig. 3 PZT patch-bonded composite beams and bluff body geometries were used in experimental studies

Table 3 RMS values of the composite beams under air load with a different type of bluff body attachment

Composite beams	Triangular-shaped bluff body (mm)	Square-shaped bluff body (mm)
$\{0°, 90°, 0°, 90°\}_s$	1.7988	2.8705
$\{-30°, 60°, -30°, 60°\}_s$	2.8209	4.2687
$\{-45°, 45°, -45°, 45°\}_s$	3.7998	4.8314

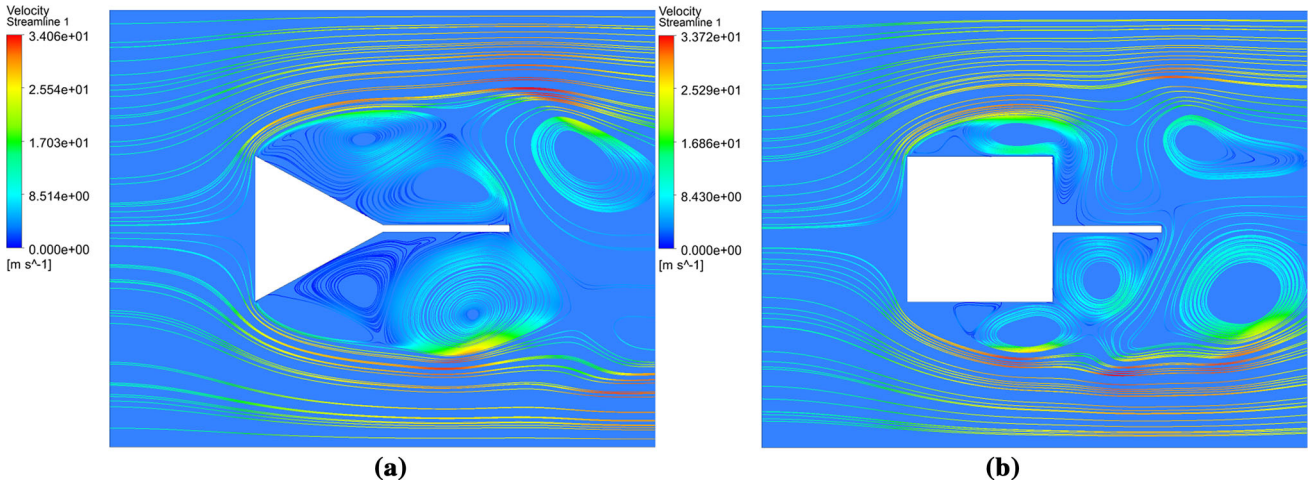

Fig. 4 Flow around the bluff body: **a** square-shaped **b** triangular-shaped

2.1 Flow-induced vibration

Bluff body geometries are connected to the beam element tips to increase the vibration amplitude obtained by the flow-induced vibration. This method is generally preferred in galloping-based energy-harvesting systems. In this study, at the same time, different bluff body geometries were investigated to increase the vibration caused by wind load on the composite beam. The time-dependent displacement responses of the aeroelastic structure were experimentally measured when these two different types of bluff-body geometries were attached to the free end of the cantilever composite beam. The displacement results are given in Table 3 as RMS values to see the uncontrolled vibration effect of different bluff body geometries on the composite beams.

The streamline obtained by the numerical method for the triangular-shaped bluff body and square-shaped bluff body used in the experimental studies is given in Fig. 4. According to the displacement results summarized in Table 3, it is seen that the square-shaped bluff body increases more the vibration on all three composite beams with each different lamination angle rather than the triangular-shaped bluff body.

To understand this situation more clearly, lift (C_l) and drag (C_d) coefficients for both bluff bodies were obtained by a numerical analysis program. C_l/C_d ratio is generally used to indicate airfoil efficiency. In this study, the lift and drag coefficients for the triangular-shaped bluff body were found as $C_l = 2.297 \times 10^{-3}$, $C_d = 0.2196$, respectively. Similarly, the square-shaped bluff body coefficients were found as $C_l = 6.356 \times 10^{-3}$, $C_d = 0.1918$, respectively. Therefore, it is seen that the C_l/C_d ratio is higher for the square-shaped bluff body, and as a result, it has an increasing effect on the vibration of the composite beam.

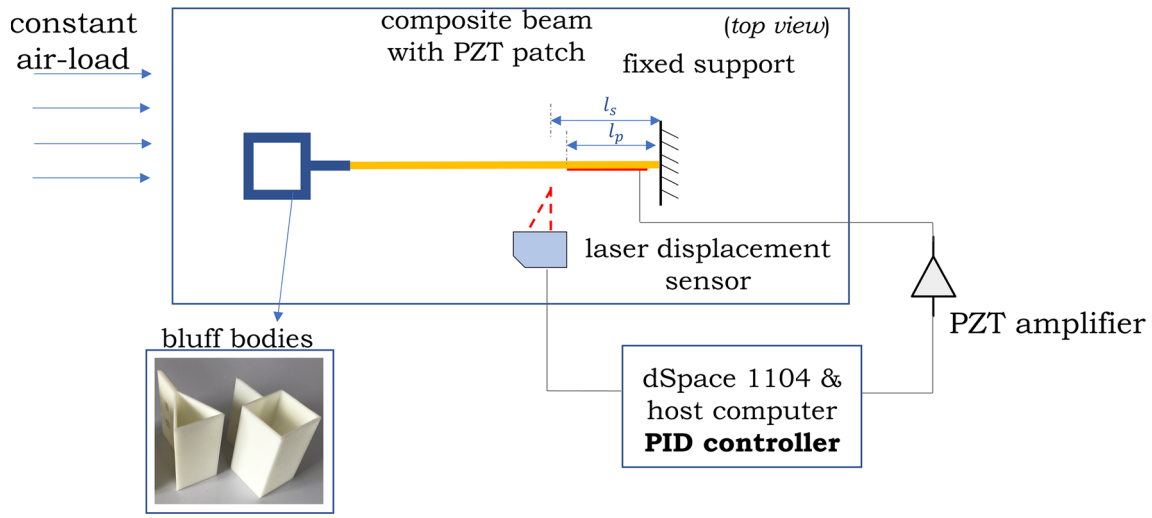

Fig. 5 Control design diagram

Fig. 6 Experimental setup

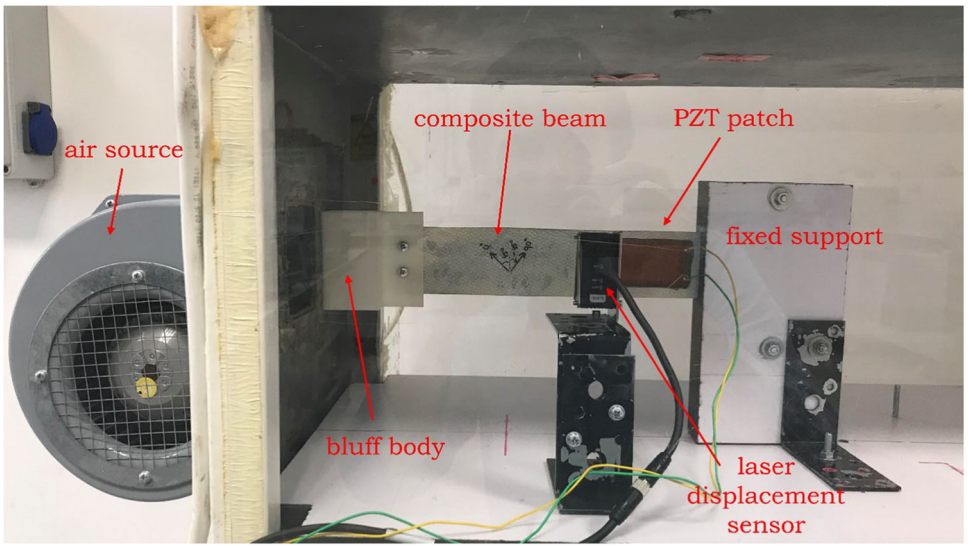

2.2 Piezoelectric-based control force

As shown in Fig. 2, when voltage is applied to the adhered piezoelectric material, it creates a bending moment effect in its region. With this moment effect, vibrations on the composite beam can be suppressed. The bending moment expression that occurs depending on the voltage magnitude calculated by the controller and transmitted to the PZT can be defined as follows.

$$M_p = -E_p d_{31} V_p b_p z_m \tag{3}$$

In here V_p and b_p represent the applied voltage and the width of the PZT actuator, respectively. Also, d_{31} represents the piezoelectric charge constant and E_p is Young's modulus of the PZT. The force due to the PZT actuator loading is derived as follows:

$$F_{\text{pzt}}(t) = \frac{M_p(t)}{I_i}\left[\psi_n'(l_i)\right] = \frac{-d_{31} E_p b_p \left(\frac{h_b+h_p}{2}\right) V_p}{\rho_b A_b {L_b}^3 + \rho_p A_p {L_p}^3}\left[\psi_n'(l_2) - \psi_n'(l_1)\right] \tag{4}$$

where h_p is the thickness of the PZT patch, h_b the thickness of the beam, b_p active width of the PZT patch, L_p length of the PZT, $\psi_n'(l_2) - \psi_n'(l_1)$ location of the PZT force, and finally M_p the bending moment.

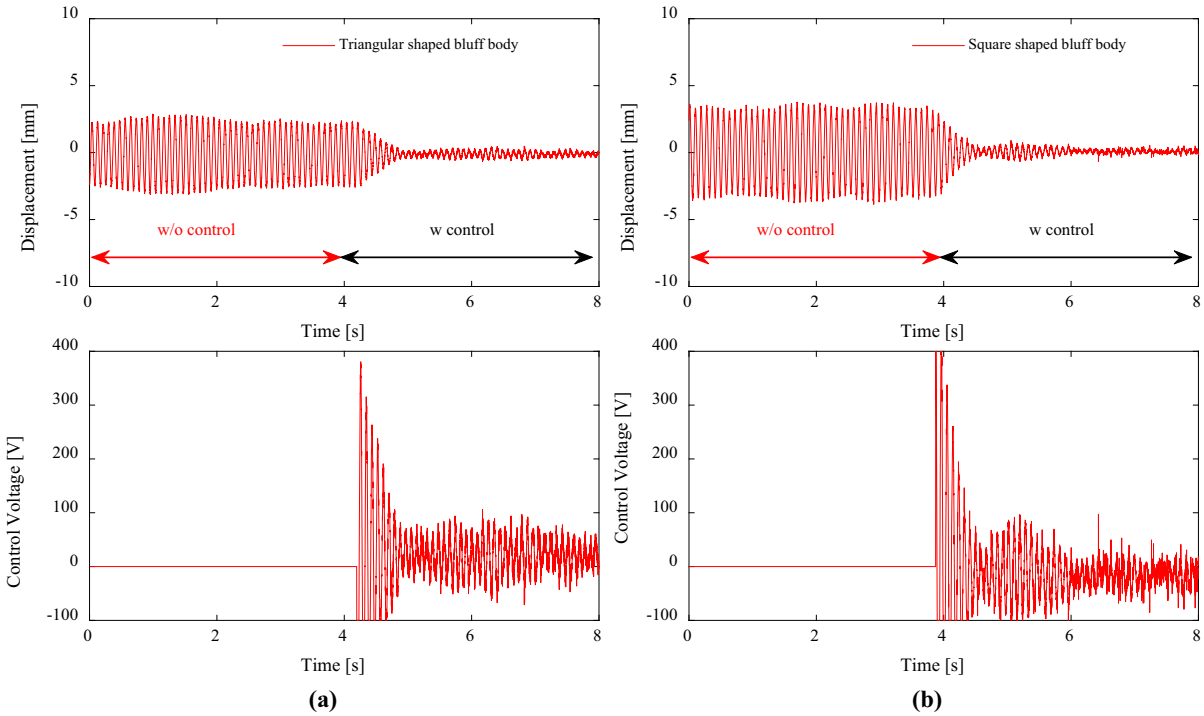

Fig. 7 **a** $\{0°, 90°, 0°, 90°\}_s$ composite beam **a** triangular-shaped bluff body displacement results under the air load and corresponding PZT control voltage and **b** square-shaped bluff body displacement results under the air load and corresponding PZT control voltage

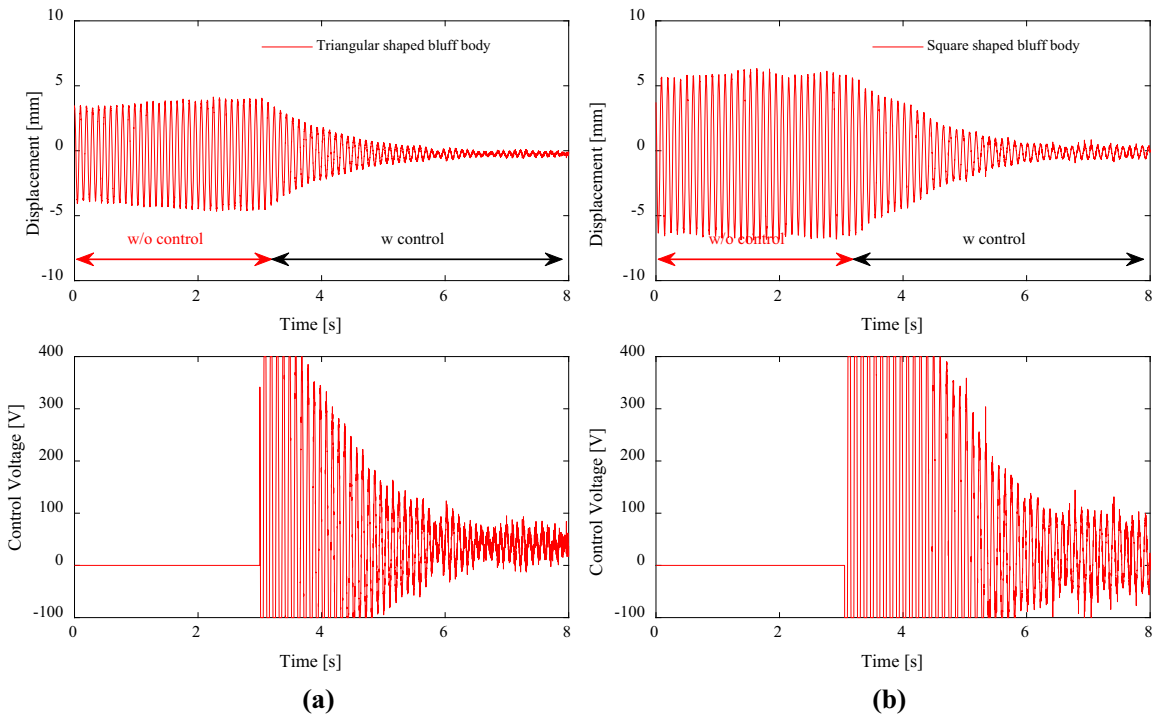

Fig. 8 **a** $\{-30°, 60°, -30°, 60°\}_s$ composite beam **a** triangular-shaped bluff body displacement results under the air load and corresponding PZT control voltage and **b** square-shaped bluff body displacement results under the air load and corresponding PZT control voltage

3 Experimental control system setup

Since composite beams with different lamination angles have their own dynamics, therefore the same control force must be applied to the beams to see the different effects of the controller. Therefore, a non-model-based PID controller design was preferred in this study.

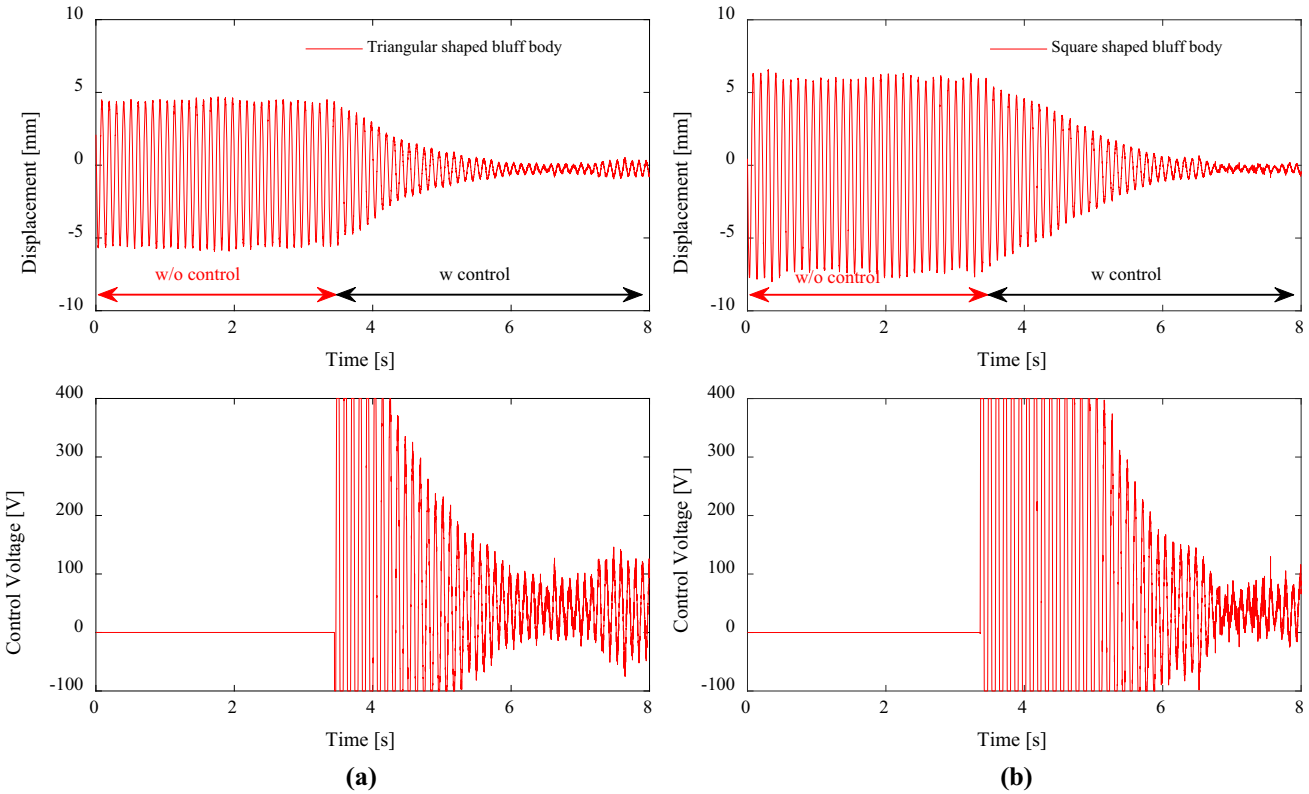

Fig. 9 $\{-45°, 45°, -45°, 45°\}_s$ composite beam **a** triangular-shaped bluff body displacement results under the air load and corresponding PZT control voltage and **b** square-shaped bluff body displacement results under the air load and corresponding PZT control voltage

Table 4 Control voltage RMS values the of the composite beams under the air-load vibration with a different type of bluff body attachment

Composite beams	Triangular-shaped bluff body (V)	Square-shaped bluff body (V)
$\{0°, 90°, 0°, 90°\}_s$	44.5213	47.9339
$\{-30°, 60°, -30°, 60°\}_s$	99.8121	131.7136
$\{-45°, 45°, -45°, 45°\}_s$	104.3996	135.4937

In this way, the influence of composite lamination angle changes has been revealed under the same controller design. The control block diagram structure designed for experimental studies of PZT patch with composite beam vibration control system is given in Fig. 5. The PID controller designed in the control studies has been applied to the system with the dSpace environment. Experimental displacement results and PZT control voltages were obtained by adding bluff bodies with square and triangular geometries to the composite beams with different lamination angles. The same PID controller was used in all experimental measurements to see the correlation between lamination angles and control efficiency and reveal the air load behavior of different bluff bodies. PID control coefficients have chosen as $P = 3$, $I = 0.5$ and $D = 0.001$. The control coefficients selected here are applied to be the same in all experimental scenarios. Therefore, the effect of active vibration control in composite beams with different lamination orientations and different bluff body attachments could be compared. The selection of the control coefficients was made in such a way as to ensure that the steady-state response converges to a fixed value (zero point) in a short period of time and would not saturate the piezoelectric patch driver circuit.

The position sensor used in the experimental studies was placed at a distance of l_s to be positioned on the front of the piezoelectric patch. Since the thicknesses of three different types of composite beams used in the experimental studies were the same, the displacement results could be compared. The piezoelectric material used is adhered to the l_p distance on the side of the fixed end of the beam to suppress the vibration. The experimental system is presented in Fig. 6. The displacement information on the flow-based cantilever beam was measured with a Keyence IL30 type laser sensor. In this system, PI's 876-A.12 type piezoelectric material has adhered to the composite beams. The piezoelectric actuator was controlled by the PI company's E413.D2 type voltage driver. This driver can supply voltage at a bandwidth of $-100 + 400$ V. dSpace 1104 card was used to transmit the time-dependent change of the displacement information and the control signal to the piezoelectric patch. Control design has been carried out in MATLAB/Simulink environment which dSpace software is communicated with it.

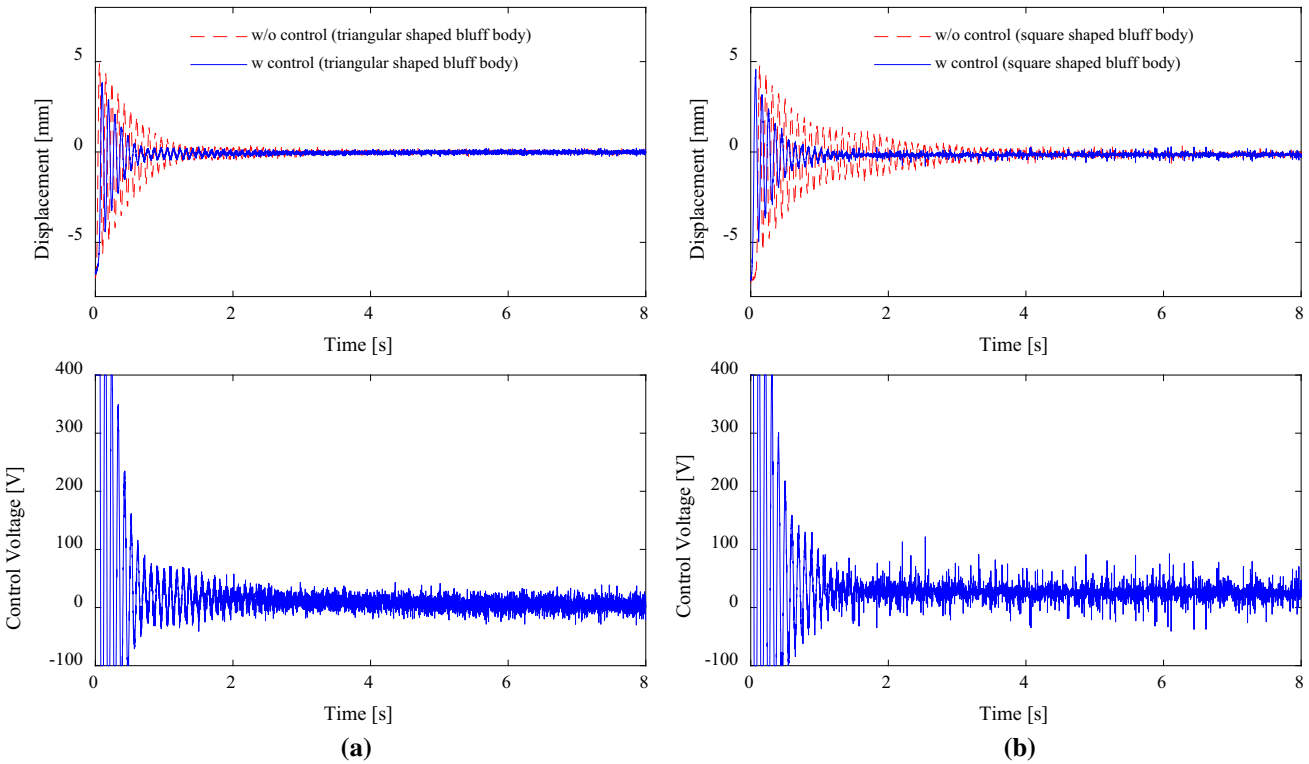

Fig. 10 $\{0°, 90°, 0°, 90°\}_s$ composite beam **a** triangular-shaped bluff body displacement results for free vibration and corresponding PZT control voltage and **b** square-shaped bluff body displacement results for free vibration and corresponding PZT control voltage

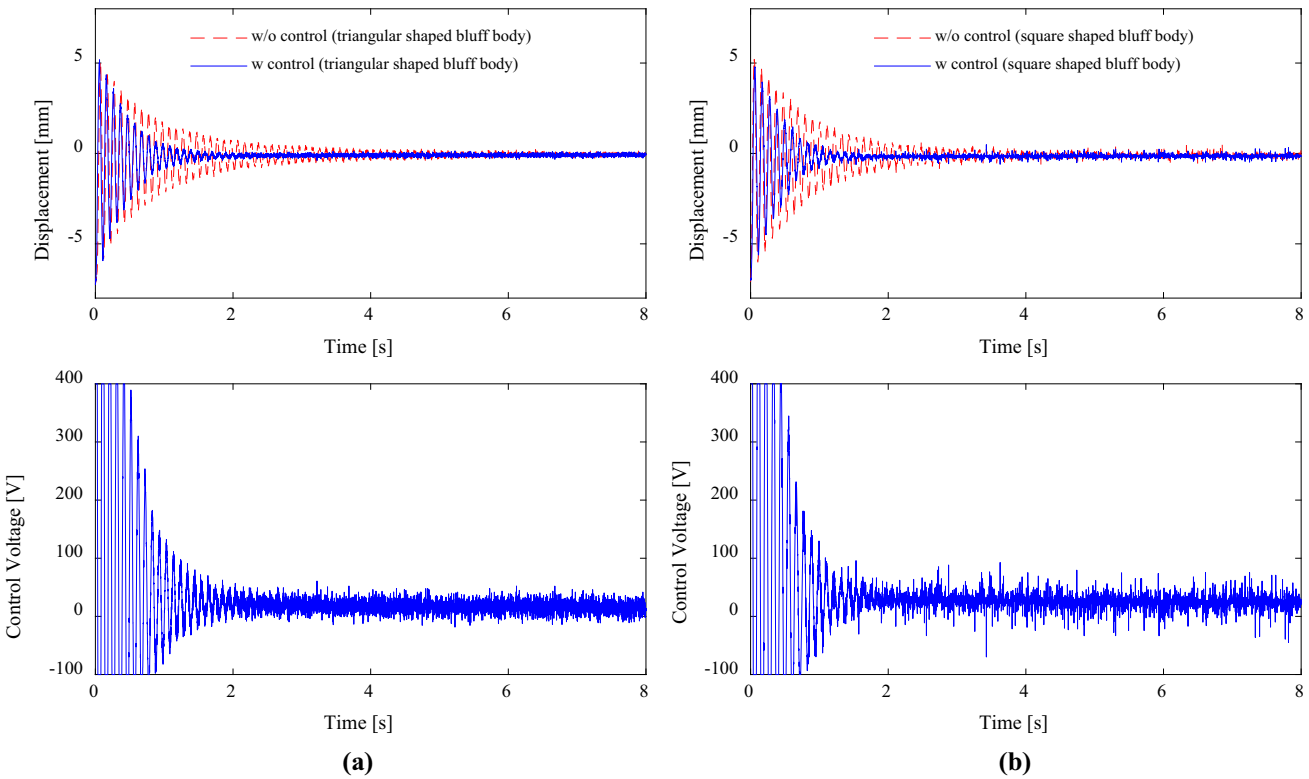

Fig. 11 $\{-30°, 60°, -30°, 60°\}_s$ composite beam **a** triangular-shaped bluff body displacement results for free vibration and corresponding PZT control voltage and **b** square-shaped bluff body displacement results for free vibration and corresponding PZT control voltage

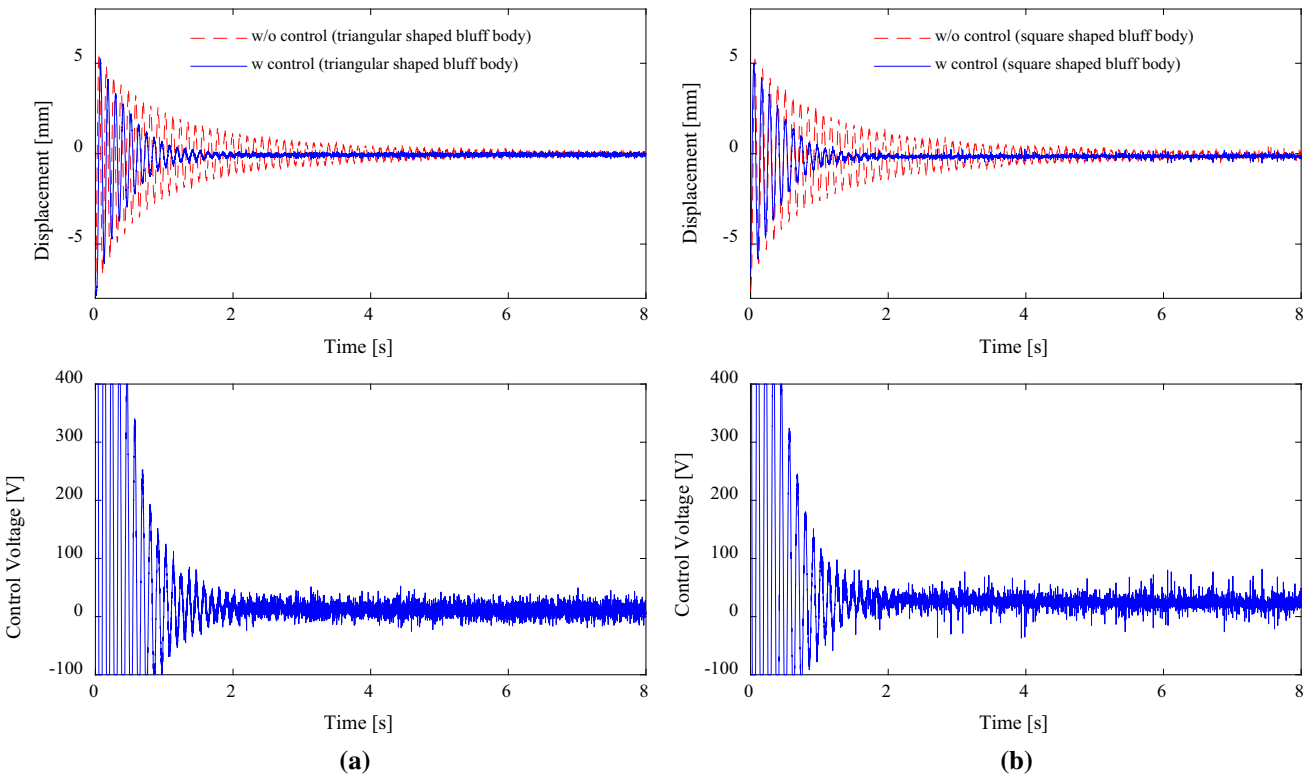

Fig. 12 $\{-45°, 45°, -45°, 45°\}_S$ composite beam **a** triangular-shaped bluff body displacement results for free vibration and corresponding PZT control voltage and **b** square-shaped bluff body displacement results for free vibration and corresponding PZT control voltage

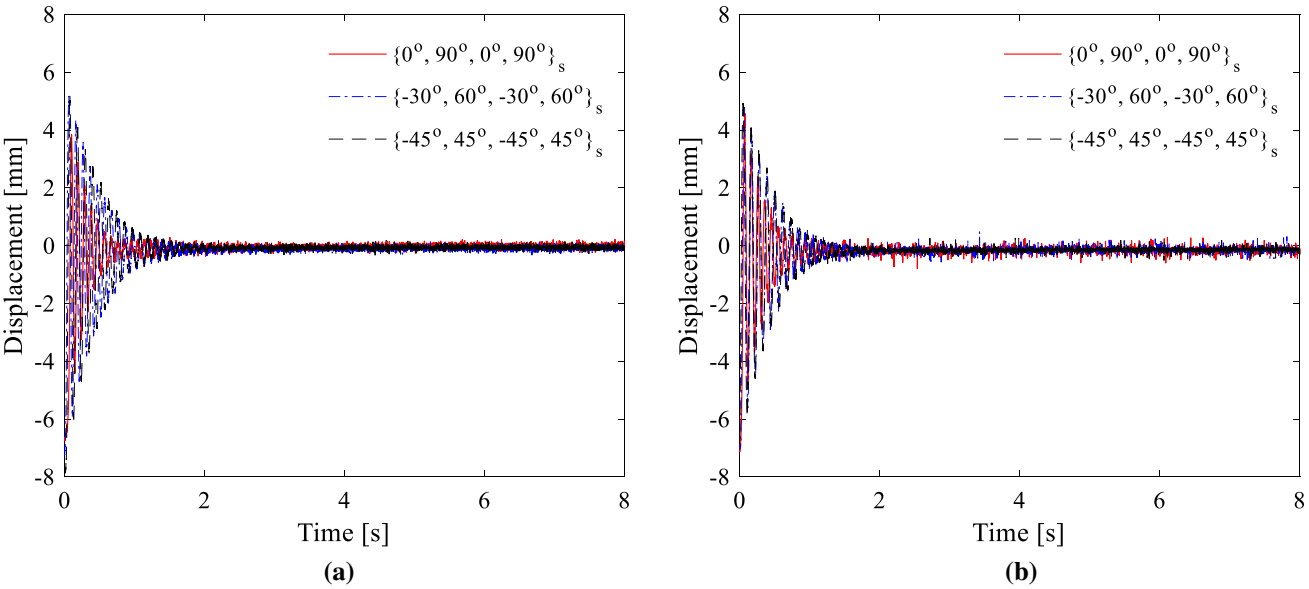

Fig. 13 Comparison of the composite beam displacement results with control effect: **a** triangular-shaped bluff body and **b** square-shaped bluff body

4 Experimental results and discussion

In this study, continuous vibration in a regular regime was obtained on a cantilever composite beam. Also, square- and triangular-shaped bluff-body geometries were attached to the composite beam end to increase the vibrations from the constant air source. Although the front surfaces of the bluff-body geometries have the same area, different magnitudes of vibrations were obtained at the same air load due to the difference in the lateral surfaces. These vibrations were measured with a laser sensor and used as a feedback

Table 5 Control voltage RMS values the of the composite beams for free vibration with a different type of bluff body attachment

Composite beams	Triangular-shaped bluff body (V)	Square-shaped bluff body (V)
$\{0°, 90°, 0°, 90°\}_s$	62.3673	66.8910
$\{-30°, 60°, -30°, 60°\}_s$	75.8377	76.1939
$\{-45°, 45°, -45°, 45°\}_s$	76.1358	77.5463

signal, and the control voltage calculated by the controller was transmitted to the piezoelectric actuator attached to the beam, and the suppression of the vibrations was realized.

The experimental results obtained in Figs. 7, 8, and 9 agree with the results given in Tables 2 and 3. The high stiffness values of the composite beams mean that it oscillates less depending on the external dynamic input with the same intensity applied. Figure 7a, b shows the controlled and uncontrolled displacement amplitudes when the triangular and rectangular bluff-body geometry is connected to the endpoint of the cantilever composite beam with $\{0°, 90°, 0°, 90°\}_s$ fiber orientation and the voltage results applied to the PTZ patch to suppress the vibrations. Figure 8a shows the displacement responses of the composite beam with $\{-30°, 60°, -30°, 60°\}_s$ lamination angle with the triangular-shaped bluff body when the control is enabled and not enabled and corresponding control voltage. Similarly, Fig. 8b shows the displacement responses of the composite beam with $\{-30°, 60°, -30°, 60°\}_s$ lamination angle with the square-shaped bluff body when the control is enabled and not enabled and corresponding control voltage. Finally, Fig. 9a, b shows the time-dependent responses of steady-state vibrations of the beam element with lamination angle $\{-45°, 45°, -45°, 45°\}_s$ and the voltage outputs required to suppress these flow-based vibrations. For better comparison, Table 4 gives the control voltages required to suppress the vibration under air load of these three composite beam vibrations for both bluff bodies.

Also, these three types of composite beam structures were released to free vibration from a certain point to determine the control performance in experimental studies. To see the initial condition responses, the vibration values of the beams and the voltage magnitudes required to suppress these vibrations were analyzed. Figures 10, 11, and 12 are the free vibration response and controlled response of composite beams with orientation of $\{0°, 90°, 0°, 90°\}_s$, $\{-30°, 60°, -30°, 60°\}_s$ and $\{-45°, 45°, -45°, 45°\}_s$, respectively. The same figures also show the corresponding control voltages applied to the PTZ patch. In Fig. 13, the triangular-shaped bluff body and square-shaped bluff body comparison of the composite beam displacement results with control effect enable are given, respectively. For better comparison, Table 5 also shows the control voltages required to suppress the free vibration responses of these three composite beam vibrations for both bluff bodies. Furthermore, the free vibration responses (Figs. 10–13) and the results obtained in Table 5 give compatible results with the stiffness coefficients of composite beams.

5 Conclusions

In this study, the control performance of cantilever composite beams with $\{0°, 90°, 0°, 90°\}_s$, $\{-30°, 60°, -30°, 60°\}_s$ and $\{-45°, 45°, -45°, 45°\}_s$ lamination angle was investigated. For this purpose, by connecting bluff-body geometries with square and triangular shape to the endpoint of the cantilever composite beams, the continuous vibration was created in a induced flow based on a regular regime. It was observed that the vibration results of the composite beam connected to the square-shaped bluff body were larger than the triangular-shaped bluff body connected beam. When the square bluff-body geometry is connected, the amplitudes of the vibrations occurring under the effect of air load without control effect are 2.87 mm for the beam with $\{0°, 90°, 0°, 90°\}_s$, orientation, 4.83 mm for the beam with $\{-30°, 60°, -30°, 60°\}_s$ orientation and finally, 4.26 mm for the beam with $\{-45°, 45°, -45°, 45°\}_s$ orientation. These results were realized following the order in which beam stiffness values were determined using a force gauge. On the other hand, the situation that arose when beam elements with these three different lamination angles were released to free vibration from a certain point has been examined. It has also been observed that the vibrations resulting from these experiments are compatible with the beam stiffness experiments. Control voltages for suppressing vibrations of three different beam elements with connected square geometry are 66.89 V for beam with $\{0°, 90°, 0°, 90°\}_s$, 76.19 V for beam with $\{-30°, 60°, -30°, 60°\}_s$ and finally 77.54 V for the beam $\{-45°, 45°, -45°, 45°\}_s$. Similarly, it was observed that the control voltage values of the composite beam connected to the square-shaped bluff body were higher than the triangle-shaped beam connected to the bluff body. As a result, while examining the control performance of composite beams with different fiber orientations, different bluff body geometries used to increase vibrations at the same time have been examined by experimental study.

Data Availability Statement This manuscript has associated data in a data repository. [Authors' comment: The data that support the findings of this study are available from the corresponding author upon reasonable request.]

Declarations

Conflict of interest On behalf of all authors, the corresponding author states that there is no conflict of interest.

References

1. Y. Pu, H. Zhou, Z. Meng, Multi-channel adaptive active vibration control of piezoelectric smart plate with online secondary path modelling using PZT patches. Mech. Syst. Signal Process. **120**, 166–179 (2019). https://doi.org/10.1016/j.ymssp.2018.10.019
2. S.S. Heganna, J.J. Joglekar, Active vibration control of smart structure using PZT patches. Proc. Comput. Sci. **89**, 710–715 (2016). https://doi.org/10.1016/j.procs.2016.06.040
3. P. Shivashankar, S. Gopalakrishnan, Review on the use of piezoelectric materials for active vibration, noise, and flow control. Smart Mater. Struct. **29**(5), 053001 (2020). https://doi.org/10.1088/1361-665X/ab7541
4. B. Tang, H. Akbari, M. Pouya, P.V. Pashaki, Application of piezoelectric patches for chatter suppression in machining processes. Measurement **138**, 225–231 (2019). https://doi.org/10.1016/j.measurement.2019.02.003
5. Z. Arabjamaloei, M. Mofidi, M. Hosseini, R. Bahaadini, Vibration analysis of rotating composite blades with piezoelectric layers in hygrothermal environment. Eur. Phys. J. Plus **134**(11), 556 (2019). https://doi.org/10.1140/epjp/i2019-12910-9
6. M. Li, F. Li, X. Jing, Active vibration control of composite pyramidal lattice truss core sandwich plates. J. Aerosp. Eng. **31**(2), 04017097 (2018). https://doi.org/10.1061/(ASCE)AS.1943-5525.0000817
7. K. Gurses, B.J. Buckham, E.J. Park, Vibration control of a single-link flexible manipulator using an array of fiber optic curvature sensors and PZT actuators. Mechatronics **19**(2), 167–177 (2009). https://doi.org/10.1016/j.mechatronics.2008.09.005
8. S.M. Kusagur, G. Arunkumar, T.C. Manjunath, Modelling of smart intelligent materials with PZT & PVDF sensors/actuators to control the active vibrations of flexible aluminum mechanical cantilever beams using proportional integral derivative (PID) techniques. Mater. Today Proc. **37**, 2075–2082 (2021). https://doi.org/10.1016/j.matpr.2020.07.507
9. M. Azimi, E.F. Joubaneh, Dynamic modeling and vibration control of a coupled rigid-flexible high-order structural system: a comparative study. Aerosp. Sci. Technol. **102**, 105875 (2020). https://doi.org/10.1016/j.ast.2020.105875
10. X. Yuan, X. Wang, M. Yan, F. Gao, S. Zhang, K. Zhou et al., Effects of composite layer thickness and driving conditions on the actuating performance of shear piezoelectric fiber composite. Measurement **154**, 107500 (2020). https://doi.org/10.1016/j.measurement.2020.107500
11. G. Takács, T. Polóni, B. Rohal-Ilkiv, Adaptive model predictive vibration control of a cantilever beam with real-time parameter estimation. Shock Vib. (2014). https://doi.org/10.1155/2014/741765
12. A. Oveisi, M. Gudarzi, Adaptive sliding mode vibration control of a nonlinear smart beam: A comparison with self-tuning Ziegler–Nichols PID controller. J. Low Freq. Noise Vib. Active Control **32**(1–2), 41–62 (2013). https://doi.org/10.1260/2F0263-0923.32.1-2.41
13. Q. Zhu, J.Z. Yue, W.Q. Liu, X.D. Wang, J. Chen, G.D. Hu, Active vibration control for piezoelectricity cantilever beam: an adaptive feedforward control method. Smart Mater. Struct. **26**(4), 047003 (2017). https://doi.org/10.1088/1361-665X/aa64c6
14. S. Sivrioglu, F.C. Bolat, E. Erturk, Active vibration control of a blade element with uncertainty modeling in PZT actuator force. J. Vib. Control **25**(21–22), 2721–2732 (2019). https://doi.org/10.1177/2F1077546319868883
15. S.H. Youn, J.H. Han, I. Lee, Neuro-adaptive vibration control of composite beams subject to sudden delamination. J. Sound Vib. **238**(2), 215–231 (2000). https://doi.org/10.1006/jsvi.2000.3081
16. E.H. Koroishi, A.W. Faria, F.A. Lara-Molina, V. Steffen, Fuzzy modal control applied to smart composite structure. J. Phys. Conf. Ser. **628**(1), 012090 (2015). https://doi.org/10.1088/1742-6596/628/1/012090
17. K. Ma, M.N. Ghasemi-Nejhad, Adaptive simultaneous precision positioning and vibration control of intelligent composite structures. J. Intell. Mater. Syst. Struct. **16**(2), 163–174 (2005). https://doi.org/10.1177/2F1045389X05048848
18. E.H. Koroishi, F.A.L. Molina, A.W. Faria, V. Steffen Junior, Robust optimal control applied to a composite laminated beam. J. Aerosp. Technol. Manag. **7**(1), 70–80 (2015). https://doi.org/10.5028/jatm.v7i1.389
19. L.H. Zheng, Y.W. Zhang, H. Ding, L.Q. Chen, Nonlinear vibration suppression of composite laminated beam embedded with NiTiNOL-steel wire ropes. Nonlinear Dyn. **103**(3), 2391–2407 (2021). https://doi.org/10.1007/s11071-021-06258-w
20. M.M. Jovanović, A.M. Simonović, N.D. Zorić, N.S. Lukić, S.N. Stupar, S.S. Ilić, Experimental studies on active vibration control of a smart composite beam using a PID controller. Smart Mater. Struct. **22**(11), 115038 (2013). https://doi.org/10.1088/0964-1726/22/11/115038
21. A.B. Shakir, A.M. Saber, Active vibration control analysis in smart composite structures using ANSYS. Revista Internacional de Métodos Numéricos para Cálculo y Diseño en Ingeniería (2020). https://doi.org/10.23967/j.rimni.2020.04.001
22. S. Varadarajan, K. Chandrashekhara, S. Agarwal, LQG/LTR-based robust control of composite beams with piezoelectric devices. J. Vib. Control **6**(4), 607–630 (2000). https://doi.org/10.1177/2F107754630000600407
23. J. Warminski, M. Bochenski, W. Jarzyna, P. Filipek, M. Augustyniak, Active suppression of nonlinear composite beam vibrations by selected control algorithms. Commun. Nonlinear Sci. Numer. Simul. **16**(5), 2237–2248 (2011). https://doi.org/10.1016/j.cnsns.2010.04.055
24. R. Rimašauskienė, V. Jūrėnas, M. Radzienski, M. Rimašauskas, W. Ostachowicz, Experimental analysis of active–passive vibration control on thin-walled composite beam. Compos. Struct. **223**, 110975 (2019). https://doi.org/10.1016/j.compstruct.2019.110975
25. X.Q. Peng, K.Y. Lam, G.R. Liu, Active vibration control of composite beams with piezoelectrics: a finite element model with third order theory. J. Sound Vib. **209**(4), 635–650 (1998). https://doi.org/10.1006/jsvi.1997.1249
26. A. Barrero-Gil, G. Alonso, A. Sanz-Andres, Energy harvesting from transverse galloping. J. Sound Vib. **329**(14), 2873–2883 (2010). https://doi.org/10.1016/j.jsv.2010.01.028